Journal of ELECTRONIC MATERIALS, Vol. 45, No. 6, 2016
DOI: 10.1007/s11664-016-4420-x
© 2016 The Minerals, Metals & Materials Society

CrossMark

Growth and Characterization of Polyimide-Supported AlN Films for Flexible Surface Acoustic Wave Devices

QI LI,[1] HONGYAN LIU,[1] GEN LI,[1] FEI ZENG,[1,4] FENG PAN[1,5]
JINGTING LUO,[2] and LIRONG QIAN[3]

1.—Key Laboratory of Advanced Materials (MOE), School of Materials Science and Engineering, Tsinghua University, Beijing 100084, China. 2.—Institute of Thin Film Physics and Applications, Shenzhen Key Laboratory of Sensor Technology, Shenzhen University, Shenzhen 518060, China. 3.—Tianjin Key Laboratory of Film Electronic and Communication Devices, School of Electronics Information Engineering, Tianjin University of Technology, Tianjin 300384, China. 4.—e-mail: zengfei@mail.tsinghua.edu.cn. 5.—e-mail: panf@mail.tsinghua.edu.cn

Highly *c*-axis oriented aluminum nitride (AlN) films, which can be used in flexible surface acoustic wave (SAW) devices, were successfully deposited on polyimide (PI) substrates by direct current reactive magnetron sputtering without heating. The sputtering power, film thickness, and deposition pressure were optimized. The characterization studies show that at the optimized conditions, the deposited AlN films are composed of columnar grains, which penetrate through the entire film thickness ($\sim 2\ \mu m$) and exhibit an excellent (0002) texture with a full width at half maximum value of the rocking curve equal to 2.96°. The film surface is smooth with a root mean square value of roughness of 3.79 nm. SAW prototype devices with a center frequency of about 520 MHz and a phase velocity of Rayleigh wave of about 4160 m/s were successfully fabricated using the AlN/PI composite structure. The obtained results demonstrate that the highly *c*-axis oriented AlN films with a smooth surface and low stress can be produced on relatively rough, flexible substrates, and this composite structure can be possibly used in flexible SAW devices.

Key words: AlN, polyimide, flexible acoustic devices, surface acoustic wave

INTRODUCTION

In the past several decades, flexible electronics have attracted tremendous interest in the fields of flat panel displays, sensors, actuators, and biomedical applications due to their lightness, flexibility, and low costs.[1–4] Flexible surface acoustic wave (SAW) devices are crucial for the development of flexible electronics as fundamental building blocks.[5] Traditional SAW devices are built on rigid substrates like single crystals of silicon,[6] $LiNbO_3$,[7] $LiTaO_3$,[8] sapphire,[9] and polycrystalline diamond films.[10] Although these substrates demonstrated good performance and have been used to fabricate SAW devices for a long time, their expanded applications are limited due to inflexibility and high costs. PI is inexpensive and possesses excellent flexibility, good chemical stability, and great mechanical and electrical properties; hence, it is extensively used in microelectronics as a flexible substrate.[11] At the same time, AlN, one of the most commonly used materials for piezoelectric films, has several advantages such as high values of relative dielectric constant (8.5) and phase velocity for the Rayleigh wave (5600 m/s) as well as excellent atmospheric stability and acid resistivity.[12] The possibility of growing high quality AlN films on PI substrates offers the opportunity of utilizing the excellent chemical and physical properties of both the AlN films and PI substrates. Thicker AlN films possess better crystal quality leading to better acoustic properties and piezoelectricity than AlN thin films. Although there are several studies of AlN

(Received June 21, 2015; accepted February 20, 2016; published online March 4, 2016)

deposition on flexible polymer substrates as listed in Table I,[4,11,13–18] little research have been conducted on the AlN thick film deposition on polyimide supports at ambient temperature for applications in SAW devices.

In this work, highly *c*-axis oriented thick AlN films were successfully deposited on PI substrates by DC reactive magnetron sputtering. The sputtering power, film thickness, and deposition pressure were optimized, and the morphology and crystal structure of the deposited films were investigated in detail. SAW prototype devices were fabricated to show the potential of using the AlN/PI composite structures in flexible SAW applications.

EXPERIMENTAL PROCEDURE

AlN thick films were prepared on the PI substrates at ambient temperature by using a DC reactive magnetron sputtering system with a 3-inch Al (99.999% pure) target. The distance between the substrates and the target was about 70 mm. Prior to insertion into the chamber, the PI substrates were subsequently degreased in acetone, ethanol, and deionized water for 4 min each followed by blow-drying in nitrogen gas. The base pressure was better than 3×10^{-5} Pa, and the sputtering atmosphere consisted of a mixture of Ar (99.999% pure) and N_2 (99.999% pure) gases with a flux ratio of 3:1. The target was pre-cleaned by argon ion bombardment for 5 min and sputtering at the deposition conditions with a closed shutter for another 5 min. The sputtering voltage was maintained at 280 V. The electrode consisted of 10 nm thick Ti and 140 nm thick Al films, which were deposited by an e-beam evaporation system with commercial target material (99.999% pure) and the base pressure below 1.19×10^{-6} Pa. The interdigital electrodes were fabricated by conventional photolithography and wet etching. The design parameters of the SAW devices are summarized in Table II.

The grain size and microstructures of the deposited AlN films were investigated by a field emission scanning electron microscope (FE-SEM) (LEO 1530) operated at 10 kV with a working distance of 5 mm. The roughness of the film was evaluated by atomic force microscopy (AFM, DI NanoMan VS) in a tapping mode. Raman scattering spectroscopy was used to assess the crystal structure of the AlN films as well as defects or possible impurities with a confocal microscope using a polarized line of 532 nm at room temperature. The texture of the AlN films was studied by x-ray diffraction (XRD) in a Bragg–Brentano configuration (θ–2θ scan) and a rocking curve (ω scan) using monochromatized Cu Kα (λ = 0.15406 nm) radiation with an operating voltage of 40 kV and a filament current of 200 mA. High resolution transmission electron microscopy (HRTEM) (Tecnai F30) was used to study the cross section of the AlN films on a-SiO_2/Si (100) substrate at an accelerating voltage of 300 kV. TEM samples of AlN on the a-SiO_2/Si (100) were prepared by mechanical polishing to a sample thickness of below 20 μm, after which ion milling was used to thin the samples to electron transparency. The acoustic properties of the AlN/PI composite structure were tested by measuring the scattering parameter S_{21} of the flexible SAW delay line with an Agilent E5071C network analyzer and a radio frequency (RF) microprobe (Cascade Microtech) equipped with a ground-signal-ground (GSG) probe.

RESULTS AND DISCUSSION

Optimization of Sputtering Parameters

In order to obtain satisfactory performance of SAW devices, it is paramount to ensure good crystal quality and high c-axial orientation of the piezoelectric films deposited on flexible substrates. The effect of deposition power, thickness, and pressure

Table II. Design parameters of the IDT electrode of the delay line SAW device

Number of IDT pairs	40
Transducer aperture	320 μm
Wavelength	8 μm
Metallization ration	0.5
Delay line	480 mm
Electrode thickness	Ti(10 nm)\Al(140 nm)

Table I. AlN on polymer substrate reported by different works

	Single (0002) texture	Thickness	FWHM of rocking curve	FWHM of θ–2θ scan
This work	Yes	2 μm	2.96°	
Ref. 13	Yes	700 nm		0.55°
Ref. 14	Yes	565 nm		0.417°
Ref. 15	No			
Ref. 16	Yes	1 μm	11.7°	
Ref. 11	Yes	700 nm		0.54°
Ref. 4	Yes	500 nm	5.1°	
Ref. 17	Yes	1 μm	8.3°	
Ref. 18	Yes	1 μm	9.1°	

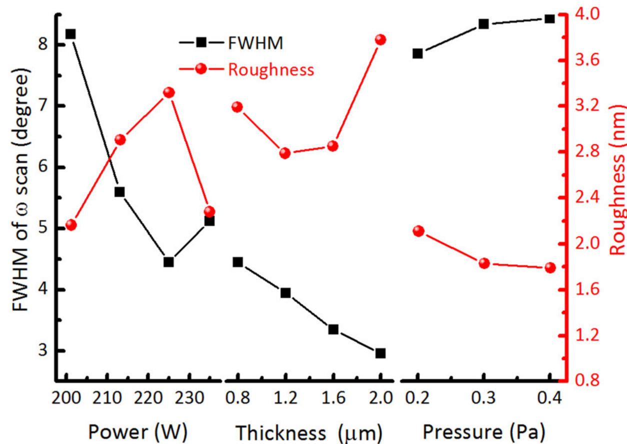

Fig. 1. The effect of sputtering power, film thickness and deposition pressure on the FWHM of the rocking curve of the AlN (0002) peak and roughness of the film. In the left part of the graph the pressure and thickness are set to 0.3 Pa and 0.8 μm; in the middle part of the picture, the power and thickness are set to 225 W and 0.3 Pa; in the right part of the picture, the power and thickness are set to 200 W and 0.8 μm.

on the properties of the AlN films was examined by varying one parameter while holding the remaining ones fixed, which led to the optimized set of the deposition parameters. The obtained results are shown in Fig. 1, where all the samples have a (0002) orientation. The FWHM of the AlN (0002) peak reaches minimum at 225 W when the sputtering power was varied between 201 W and 235 W. The sputtering power values lower than 225 W result in decreased kinetic energy of the incident atoms, and, therefore, inability to rearrange themselves.[12] When the sputtering power is greater than 225 W, the high-energy incident atoms destroy the newly formed AlN layer and reduce the adatom diffusion length, thus deteriorating the (0002) orientation.[19] Since PI substrates have low acoustic velocity without piezoelectricity, the AlN films deposited on those substrates have to be thick enough to ensure good acoustic properties and piezoelectricity. The FWHM of the AlN (0002) rocking curve monotonously decreases with an increase in the AlN film thickness, which may be due to the large amount of defects such as dislocations, stacking faults, grain boundaries, or even amorphousness at an early stage of the film growth. The *c*-axis oriented grains grow faster than the grains with other orientations; therefore, thicker films have a larger fraction of the *c*-axis oriented film resulting in a smaller FWHM of the rocking curve as reported in Ref. 20. The deposition pressure was varied between the fixed 0.2 Pa, 0.3 Pa, or 0.4 Pa values to investigate its effect on the film crystal structure. In this range, the FWHM of the AlN (0002) rocking curve increases with the deposition pressure. On the one hand, low deposition pressure reduces collisions between incident atoms, which now have enough energy to migrate on the surface of the substrate to form the (0002) AlN films with the lowest energy;[12] on the other hand, low deposition pressure leads to instability of the deposition process. In order to obtain a high degree of orientation and, thus, a high electromechanical coupling coefficient for a piezo film, the AlN film was deposited with a sputtering power of 225 W, a deposition pressure of 0.3 Pa, and a thickness of 2 μm. The sample was systematically analyzed to investigate AlN/PI composite structure with the SEM, AFM, Raman, XRD, and TEM. For the SAW prototype devices' characterization, 6.2 μm thick AlN films were used to ensure good piezoelectricity and acoustic properties.

Morphology

Since SAWs are known to propagate along the surface and almost all their energy is confined within a wavelength from the surface to the inside; hence, surface roughness greatly affects device performance.[21] Therefore, it is important to examine the morphology of the AlN films deposited on the PI substrate. Figure 1 shows the roughness values at different deposition parameters indicating an apparent mismatch between the optimal values of FWHM and roughness. As the FWHM parameter is more critical for obtaining a strong signal in the device applications, the sample of 2 μm thickness with a little bit larger RMS value is chosen for AFM and SEM. Figure 2a shows the FE-SEM image of the of the AlN film cross-section indicating that the AlN film consists of a lot of columnar grains, which are perpendicular to the PI substrate surface and penetrate through the entire film. The film microstructure is dense and crack-free with no voids between the grains. There are numerous fine columnar grains with a width of only about several nanometers at the interface between the substrate and the AlN film, while the columnar grain size increases near the surface due to the merges between the smaller grains located under the larger grains. The larger grains result in better crystallinity, but also produce a rough surface when randomly oriented. The surface morphology measured by AFM reveals that the as-prepared AlN films possess a relatively smooth surface with an RMS roughness (Rq) of $\sim$3.79 nm over the 2 μm $\times$ 2 μm surface area. Compared with the AlN film deposited on an ordinary rigid polished substrate at a relatively high temperature, such surface morphology may result from the low mobility of adatoms at low temperatures and the poor surface quality of the PI substrate. The obtained results show that the AlN columnar grains can grow well on the PI substrates and have a surface flat enough to satisfy the requirements of the SAW device fabrication.

Crystal Structure and Stress

Raman microscopy is a nondestructive method for crystal structure characterization, which is very

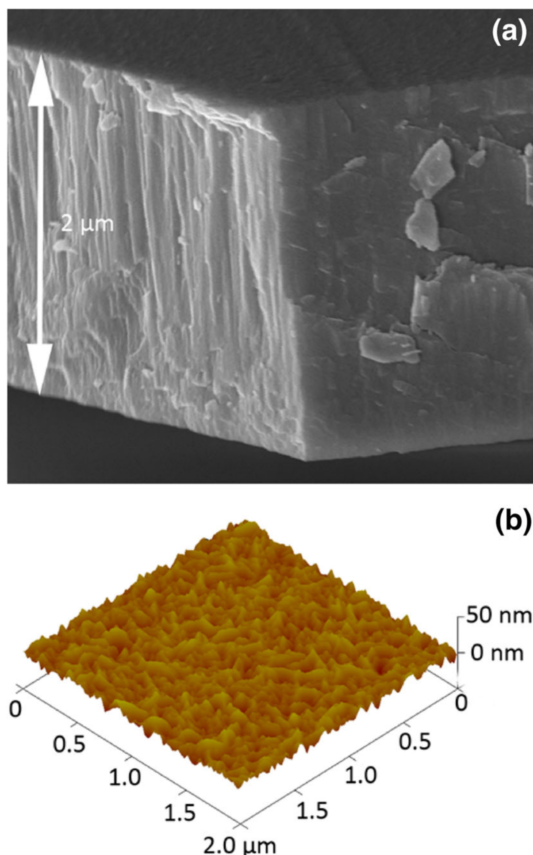

Fig. 2. (a) FE-SEM image of the cross-sectional of the AlN film, (b) surface morphology of AlN film measured by AFM under tapping mode. The roughness RMS value is 3.79 nm.

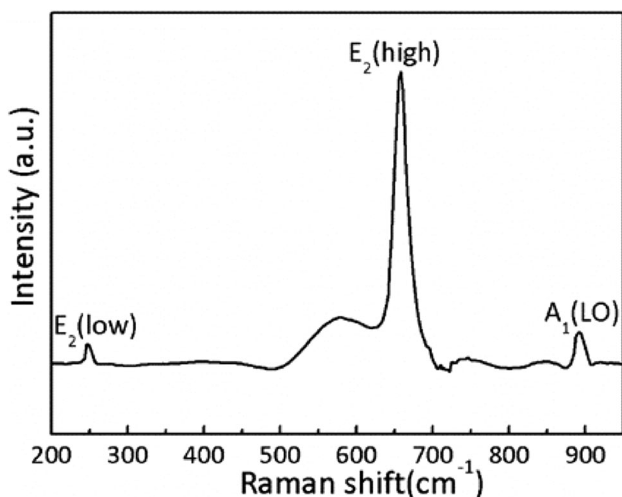

Fig. 3. Raman spectrum of the AlN film on PI substrate.

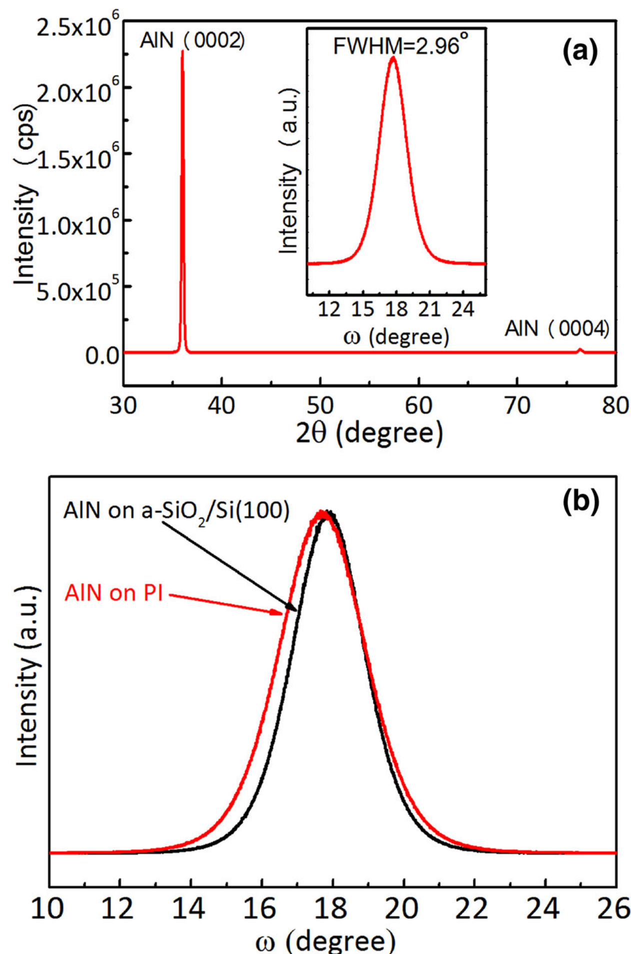

Fig. 4. (a) XRD pattern of the as-prepared AlN film on PI substrate. The corresponding rocking curve for the AlN (0002) diffraction peak is shown in the inset, (b) the rocking curves of the AlN (0002) diffraction peak on a-SiO_2/Si(100) substrate and PI substrate with intensity normalized for comparison.

sensitive to disorders and residual strains. Wurtzite AlN belongs to the space group C_{6v}^4 and is known to have a hexagonal unit cell with two lattice parameters, a and c. It is composed of two interpenetrating hexagonal close-packed sublattices, with each sublattice containing four atoms per primitive cell. According to group theory, zone-center optical phonons can be decomposed using the formula: $\Gamma_{opt} = A_1 + 2B_1 + E_1 + 2E_2$. Among these modes, the two E_2 modes marked as E_2 (high) and E_2 (low) are both Raman and infrared active, while the two B_1 modes are Raman silent. Since the A_1 and E_1 modes are polar, they can split into the longitudinal optical (LO) and transverse optical (TO) components; and the branches of the A_1 and E_1 modes, in which the phonons are polarized in the z direction and along the x–y plane, respectively, are also Raman silent.[22] In this study, a backscattering configuration was used with the Z direction perpendicular to the film surface. Figure 3 depicts a typical Raman spectrum of the AlN film. The peak at 658 cm^{-1} corresponds to the E_2 (high) mode of AlN, the strongest of the allowed modes for the c-axis oriented wurtzite film in the backscattering configuration. This value is slightly larger than 657.4 ± 0.2 cm^{-1}[23] in the zero-stress state resulting

in small compression under the internal stress of about -162 ± 54 MPa according to Ref. 24. In addiiton, the FWHM of the E_2 (high) mode is 23 cm^{-1}, between 3 cm^{-1} for AlN bulk single crystals of the highest quality and 50 cm^{-1} for highly defective crystals, which may be due to changes in phonon frequencies and lifetimes. This indicates that even though the texture of the film is good (as shown in Fig. 4a), some defects (such as point defects, dislocations, and grain boundaries) still exist on the surface. The other two predicted peaks for this configuration are E_2 (low) at 246 cm^{-1} and A_1 (LO) at 892 cm^{-1}. These three coexisting Raman peaks predicted by the selection rules indicate that the deposited AlN films have the wurtzite structure with the c-axis orientation perpendicular to the substrate surface. The peak at 578 cm^{-1} is attributed to the PI substrate, since it can also be detected on the bare PI substrate without the AlN film. The absence of either disorder-activated Raman scattering generally associated with the lattice disorder or local vibrational modes generally associated with substitutional impurities is an indication of the overall good quality of the deposited AlN films and the absence of impurities.[24]

Since trace amounts of non-(0002) planes parallel to the substrate surface in the AlN film can result in the degradation of piezoelectric response and have a major impact on the SAW device performance,[25] the texture of the deposited AlN films was analyzed by XRD. θ–2θ scans collect the x-rays diffracted only from the planes of the film, which are parallel to the substrate surface. A typical XRD (θ–2θ scan) pattern of the AlN/PI composite structure is shown in Fig. 4a. Only the peaks at 36.00° and 76.36° were detected. The peak intensities are quite strong, with the peak at 36.00° corresponding to the (0002) diffraction peak of wurtzite AlN, which indicates a strongly oriented (0002) texture. In addition, the rocking curve for this plane is obtained to further examine the AlN film texture. The inset of Fig. 4a shows a low FWHM value of 2.96°, which is satisfactory considering that the AlN films were deposited on a relative rough PI substrate directly by DC reactive magnetron sputtering without heating. Generally, higher adatom mobility promotes the growth of the AlN thin films with a c-axis orientation, since, if the particles have higher mobility, they are more likely to occupy the low energy binding sites leading to faster crystal growth in the planes with highest surface energy (in this case, the (0002) plane). Figure 2a shows a larger number of fine grains in the first thin bottom layer of the film due to the amorphousness of the substrate. There is no coherence between the substrate and the deposited film, so the c-axis of these fine grains can deviate from the substrate surface normal leading to the spread in orientation. In addition, a rough substrate surface with an RMS roughness of 1.52 nm and a high deposition rate of about 20 nm/min can also lead to low adatom mobility. At low temperatures, the growth of the AlN films is considered thermodynamically limited due to the low thermal energy for sufficient adatom mobility. There are some works[26,27] about the impact of the substrate roughness on the FWHM of the AlN (0002) rocking curve at low temperatures. These studies are focused on the migration energy of the adatoms originating from the kinetic energy of sputtered particles, which is sufficient for moving only across a very smooth surface due to the low substrate temperature. On rough surfaces, AlN also nucleates along the (0002) plane parallel to the local surface. However, there is a tilt variation from grain to grain impeding the cumulative c-axis orientation. As the substrate roughness increases, the film texture gradually degrades. There is a large difference in substrate roughness between PI and a-SiO_2/Si (100) as shown in Table III, but the difference in FWHM of the AlN (0002) rocking curves for these two substrates is relatively small compared to the previous works.[27] Highly c-axis oriented AlN films can be deposited on such rough amorphous substrates opening an opportunity for this AlN/PI composite structure to be used in SAW device applications.

Figure 4b displays the two rocking curves for the AlN films deposited on the a-SiO_2/Si(100) and PI substrates using the same deposition process. The substrate thermal expansion coefficient,[28,29] substrate roughness, AlN film roughness, FWHM, and 2θ of the AlN (0002) diffraction peak, and internal stress for the deposited AlN films on PI and a-SiO_2/Si(100) are listed in Table III. The internal stress σ_{film} parallel to the film surface was calculated according to the following equation:

$$\sigma_{\text{film}} = \frac{2c_{13}^2 - c_{33}(c_{11} + c_{12})}{2c_{13}} \times \frac{(c_{\text{film}} - c_{\text{th}})}{c_{\text{th}}}, \qquad (1)$$

where c_{11},c_{12},c_{13} and c_{33} are the stiffness constants for AlN,[30] c_{film} and c_{th} are the experimental and theoretical lattice parameters c for the AlN films, respectively. As seen in Fig. 4b, the (0002) diffraction peak value for AlN deposited on the PI substrate shifts toward the lower 2θ angle compared with that on the a-SiO_2/Si(100) substrate, and both of them are smaller than the standard value of the AlN powder. It means that both deposited AlN films undergo compressive stress, though it is relatively small as shown in Table III. This small residual compressive stress most likely results from the deposition at low sputtering pressures, when the ejected Al particles with higher kinetic energies (due to an increased mean free path of the sputtered particles with little scattering) bombard the as-grown film at an angle approximately normal to the surface leading to dissociation of loosely packed planes and decreasing voids. Hence, a dense and compact film was formed under compressive stress. In addition, the AlN film on the PI substrate has larger in-plane compressive stress than the AlN film

Table III. Comparisons of samples deposited on PI and a-SiO$_2$/Si(100)

	PI	a-SiO$_2$/Si (100)
$\alpha_{substrate}$	20×10^{-6} K^{-1}[28]	2.69×10^{-6} K^{-1}[29]
Rq$_{substrate}$ (nm)	1.55	0.19
Rq$_{AlN}$ (nm)	3.79	2.70
FWHM	2.95°	2.50°
2θ	36.00°	36.02°
σ_{film} (MPa)	−827	−473

grown on the a-SiO$_2$/Si(100) substrate. The difference in the quantity of stress is likely due to a thermal expansion coefficient mismatch. The thermal expansion coefficient of AlN is located between the corresponding values for PI and a-SiO$_2$/Si(100) as listed in Table III. If both composite structures undergo the same temperature change, the AlN film on PI will exhibit compressive stress, while the AlN film on a-SiO$_2$/Si(100) will be under tensile stress. Finally, a combination of thermal stress with Al particle bombardment can explain why the AlN film grown on the PI substrate undergoes bigger compressive stress than the AlN film deposited on the a-SiO$_2$/Si(100) substrate. In general, the parameters of the AlN film deposited on PI are almost comparable with those for the AlN film prepared on the a-SiO$_2$/Si (100) substrate (see Table III).

Voids and cracks not only affect the acoustic velocity and electromechanical coefficient of a material, but also result in a transmission loss. Conventional and high-resolution TEM analysis were used to examine the cross-sectional microstructures on amorphous substrates. A cross-sectional sample of AlN on the a-SiO$_2$/Si(100) substrate was manufactured, since it is difficult to prepare a cross-sectional sample of AlN on the PI substrate. A representative low magnification cross-sectional TEM image of the AlN/a-SiO$_2$/Si(100) composite structure is shown in Fig. 5a, where the AlN and a-SiO$_2$ film thicknesses are 2 μm and 300 nm, respectively. The thickness of the obtained AlN film is in good agreement with the AlN films deposited on the PI substrate using the same process (as shown in Fig. 2a). The film consists of highly parallel columnar grains similar to those observed for the films deposited on the PI substrate. Figure 5b shows a typical HRTEM image that reveals a transitional thin interlayer between AlN and the amorphous SiO$_2$, which is similar to the one reported earlier.[31] This amorphous interlayer is most likely formed in the beginning of the deposition process when the substrate temperature is low. A high deposition rate of 20 nm/min and a low substrate temperature make it difficult for the adatoms to rearrange themselves and crystallize well. A selected area electron diffraction (SAED) pattern for the AlN/a-SiO$_2$ interface with a field view of ~200 nm is presented in the inset of Fig. 5b.

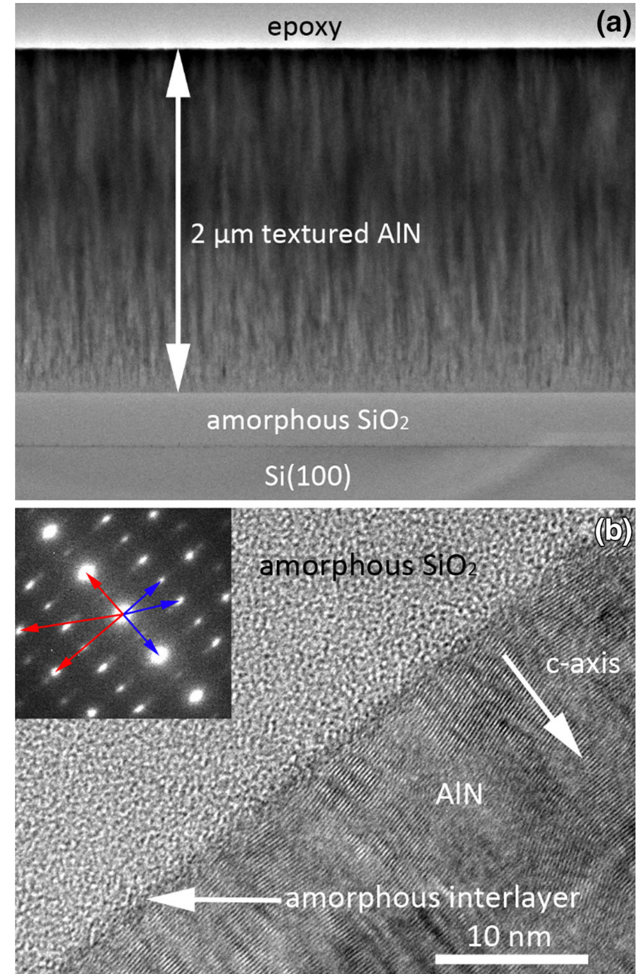

Fig. 5. (a) Cross-sectional TEM image of 2 μm thick AlN film on the a-SiO$_2$/Si(100) substrate, (b) cross-sectional HRTEM image of the interface between AlN and amorphous SiO$_2$. Inset in (b) is SAED pattern of 2 μm AlN grown on 300 nm amorphous SiO$_2$.

There are two sets of diffraction spots as shown in the inset. The spots marked by a blue arrow belong to the crystal zone of $[2\bar{1}\bar{1}0]$, while the spots marked by a red arrow belong to the crystal zone of $[10\bar{1}0]$. These two domains locally rotate 30° with respect to each other along the *c*-axis, though they are randomly distributed over the whole film. In fact, several SAED patterns collected at different spots of the AlN film cross-section were almost identical. These results support the conclusion that the AlN grains on the amorphous substrate are well textured along the [0001] direction. Since both the PI and a-SiO$_2$/Si(100) substrates are amorphous, and the quality of the deposited AlN films is about the same (as indicated by the XRD results),we may roughly know the AlN microstructures on the PI substrate can be assessed qualitatively.

Prototype Device Characterization

Using the obtained data, highly *c*-axis oriented device-grade AlN films were successfully prepared

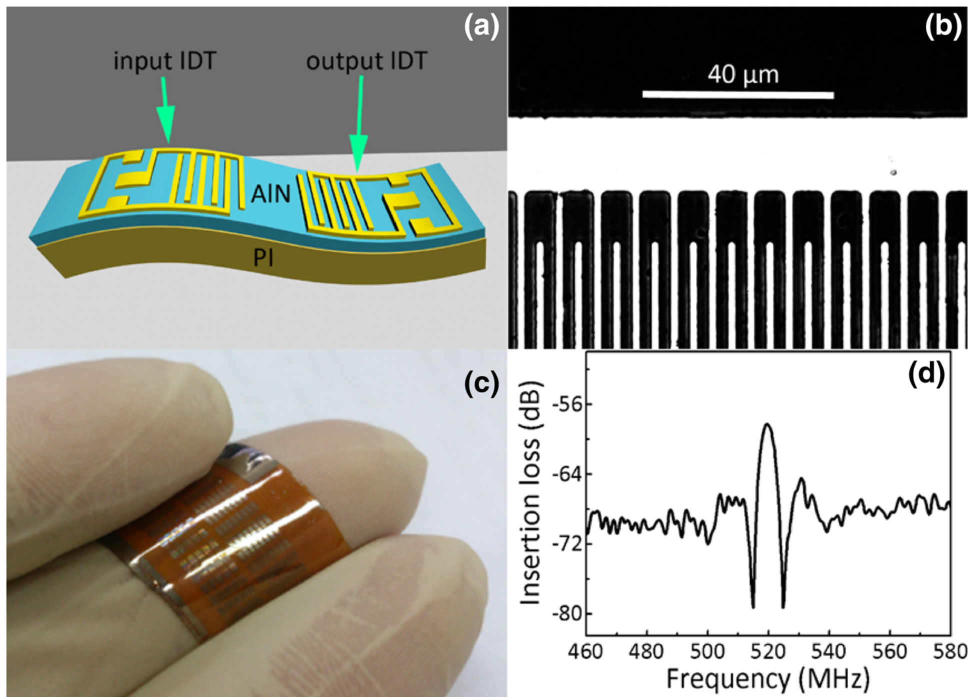

Fig. 6. (a) Schematic of the developed flexible SAW delay line device on AlN/PI composite structure, (b) microscope image of interdigital transducer fingers, (c) photographs of flexible SAW delay line devices on PI substrate, and (d) frequency response of the flexible SAW delay line device.

on PI substrates by DC reactive magnetron sputtering at ambient temperature. The fabricated delay line devices are schematically shown in Fig. 6a. In these devices, SAW propagates in the direction normal to the *c*-axis of the AlN film in order to demonstrate the practical operation of the piezoelectric AlN films grown on the PI substrates. The manufactured devices consist of Al (140 nm), Ti (10 nm), and AlN (6.2 μm) layers deposited on PI (125 μm) substrates. The Ti underlayer is used to enhance the adhesion between the Al and AlN layers. The PI substrate ensures that the device is light and flexible, while the 6.2-μm AlN layer with a rocking curve FWHM of 2.45° and RMS value of 4.9 nm ensures that the AlN film used to fabricate SAW devices has good piezoelectricity, and that the resultant SAW delay line devices perform well in acoustoelectric conversion. An electrical signal is input into the device via an input interdigital transducer (IDT) followed by its transformation into an acoustic signal via the converse piezoelectric effect of the AlN film, which transmits sound waves along the film surface. Finally, it is converted back into an electrical signal via an output IDT by the piezoelectric effect. Figure 6b shows a microscope image of the IDT fingers on the AlN/PI composite structure having the same width a with finger space of 2 μm, which is essential for good performance. The fabricated SAW delay line device shown in Fig. 6c is characterized by high flexibility.

Figure 6d plots a typical frequency response of the device after time-gating, which was employed to remove the electromagnetic feedthrough effect. It clearly indicates that a flexible SAW delay line device with a center frequency of 520 MHz was successfully fabricated. Since the sensitivity of a SAW device is known to be proportional to its center frequency, the fabricated flexible SAW device with high center frequency of 520 MHz is promising for all sorts of highly sensitive sensors.[32–34] The phase velocity of the excited SAW was estimated by using the following equation:

$$v = \lambda \times f_0, \quad (2)$$

where λ is the IDT periodicity (equal to 8 μm) and f_0 is the center frequency of the fabricated device. According to this formula, the phase velocity of the fabricated device can be calculated as $v = \lambda \times f_0 = 8\,\mu\text{m} \times 520\,\text{MHz} = 4160\,\text{m/s}$. Such a high phase velocity of Rayleigh wave is reasonable considering that, on the one hand, the thickness of the deposited AlN film is 6.2 μm with a relatively large film thickness ratio h/λ equal to 0.75. On the other hand, AlN has a very high phase velocity of Rayleigh wave of about 5600 m/s. These two factors may have contributed to the high values of both the phase velocity and center frequency of the deposited AlN films. A relatively high insertion loss of this prototype device is probably due to the large FWHM value of the rocking curve.[35] It can be improved in the future by adding a transition layer[14] on a proper substrate or by design optimization.[36] A proper substrate may be obtained by using pre-deposition

RF plasma etching[37] or another material, which requires further studies. In general, the obtained results indicate that the manufactured AlN/PI composite structures are suitable for flexible SAW device fabrication.

CONCLUSIONS

In this study, highly *c*-axis oriented AlN films were successfully deposited on relatively rough PI substrates by DC reactive magnetron sputtering at a total pressure of 0.3 Pa and a sputtering power of 225 W. The as-prepared 2 μm thick AlN films have a high *c*-axis orientation with the FWHM of the rocking curve equal to 2.96° and consist of multiple highly ordered columnar grains penetrating through the entire film thickness. The prototype devices with a center frequency of about 520 MHz and a high phase velocity of Rayleigh wave of about 4160 m/s were fabricated to demonstrate the great potential of the AlN/PI composite structures to be used in flexible SAW devices.

ACKNOWLEDGEMENTS

This work was supported by the National Natural Science foundation of China (Grant Nos. 51371103 and 51231004), National Basic Research Program of China (Grant No. 2010CB832905) and National Hi-tech (R&D) project of China (Grant Nos. 2012AA03A706, 2013AA030801), and the Research Project of Chinese Ministry of Education (No 113007A).

REFERENCES

1. Y. Sun and J.A. Rogers, *Adv. Mater.* 19, 1897 (2007).
2. X. He, D. Li, J. Zhou, W. Wang, W. Xuan, S. Dong, H. Jin, and J. Luo, *J. Mater. Chem. C* 1, 6210 (2013).
3. S. Petroni, G. Maruccio, F. Guido, M. Amato, A. Campa, A. Passaseo, M.T. Todaro, and M. De Vittorio, *Microelectron. Eng.* 98, 603 (2012).
4. N. Jackson, L. Keeney, and A. Mathewson, *Smart Mater. Struct.* 22, 115033 (2013).
5. H. Jin, J. Zhou, X. He, W. Wang, H. Guo, S. Dong, D. Wang, Y. Xu, J. Geng, J.K. Luo, and W.I. Milne, *Sci. Rep.* 3, 2140 (2013).
6. C. Caliendo, P. Imperatori, and E. Cianci, *Thin Solid Films* 441, 32 (2003).
7. K.S. Kao, C.C. Cheng, Y.C. Chen, and C.H. Chen, *Appl. Surf. Sci.* 230, 334 (2004).
8. R. Rimeika, A. Sereika, and D. Čiplys, *Appl. Phys. Lett.* 98, 052909 (2011).
9. T. Aubert, M.B. Assouar, O. Legrani, O. Elmazria, C. Tiusan, and S. Robert, *J. Vac. Sci. Technol. A* 29, 021010 (2011).
10. C.C. Sung, Y.F. Chiang, R. Ro, R. Lee, and S. Wu, *J. Appl. Phys.* 106, 124905 (2009).
11. S. Petroni, C. La Tegola, G. Caretto, A. Campa, A. Passaseo, M. De Vittorio, and R. Cingolani, *Microelectron. Eng.* 88, 2372 (2011).
12. H.Y. Liu, G.S. Tang, F. Zeng, and F. Pan, *J. Cryst. Growth* 363, 80 (2013).
13. S. Petroni, F. Guido, B. Torre, A. Falqui, M.T. Todaro, R. Cingolani, and M. De Vittorio, *Analyst* 137, 5260 (2012).
14. H. Jin, J. Zhou, S.R. Dong, B. Feng, J.K. Luo, D.M. Wang, W.I. Milne, and C.Y. Yang, *Thin Solid Films* 520, 4863 (2012).
15. S.G. Yang, A.B. Pakhomov, S.T. Hung, and C.Y. Wong, *Appl. Phys. Lett.* 81, 2418 (2002).
16. M. Akiyama, Y. Morofuji, T. Kamohara, K. Nishikubo, M. Tsubai, O. Fukuda, and N. Ueno, *J. Appl. Phys.* 100, 114318 (2006).
17. M. Akiyama, Y. Morofuji, T. Kamohara, K. Nishikubo, Y. Ooishi, M. Tsubai, and N. Ueno, *Adv. Funct. Mater.* 17, 458 (2007).
18. M. Akiyama, Y. Morofuji, K. Nishikubo, and T. Kamohara, *Appl. Phys. Lett.* 92, 043509 (2008).
19. K.-H. Chiu, J.-H. Chen, H.-R. Chen, and R.-S. Huang, *Thin Solid Films* 515, 4819 (2007).
20. F. Martin, P. Muralt, M.A. Dubois, and A. Pezous, *J. Vac. Sci. Technol. A* 22, 361 (2004).
21. X.H. Xu, H.S. Wu, C.J. Zhang, and Z.H. Jin, *Thin Solid Films* 388, 62 (2001).
22. H. Liu, F. Zeng, G. Tang, and F. Pan, *Appl. Surf. Sci.* 270, 225 (2013).
23. T. Prokofyeva, M. Seon, J. Vanbuskirk, M. Holtz, S. Nikishin, N. Faleev, H. Temkin, and S. Zollner, *Phys. Rev. B* 63, 125313 (2001).
24. V. Lughi and D.R. Clarke, *Appl. Phys. Lett.* 89, 241911 (2006).
25. A.P. Huang, G.J. Wang, S.L. Xu, M.K. Zhu, G.H. Li, B. Wang, and H. Yan, *Mater. Sci. Eng. B* 107, 161 (2004).
26. S.H. Lee, J.K. Lee, and K.H. Yoon, *J. Vac. Sci. Technol. A* 21, 1 (2003).
27. A. Artieda, M. Barbieri, C.S. Sandu, and P. Muralt, *J. Appl. Phys.* 105, 024504 (2009).
28. DuPont™ Kapton® HN polyimide film Technical Data Sheet. http://www.dupont.com/content/dam/assets/products-and-services/membranes-films/assets/DEC-Kapton-HN-datasheet.pdf. Accessed 25 May 2015.
29. Y. Okada and Y. Tokumaru, *J. Appl. Phys.* 56, 314 (1984).
30. A.F. Wright, *J. Appl. Phys.* 82, 2833 (1997).
31. C.M. Lin, W.C. Lien, V.V. Felmetsger, M.A. Hopcroft, D.G. Senesky, and A.P. Pisano, *Appl. Phys. Lett.* 97, 141907 (2010).
32. S. Wenzel and R. White, *Appl. Phys. Lett.* 54, 1976 (1989).
33. J.T. Luo, P.X. Luo, M. Xie, K. Du, B. Zhao, F. Pan, P. Fan, F. Zeng, D. Zhang, Z. Zheng, and G. Liang, *Biosens. Bioelectron.* 49, 512 (2013).
34. F. Di Pietrantonio, M. Benetti, V. Dinca, D. Cannatà, E. Verona, S. D'Auria, and M. Dinescu, *Appl. Surf. Sci.* 302, 250 (2014).
35. C.-M. Lin, T.-T. Yen, Y.-J. Lai, V.V. Felmetsger, M.A. Hopcroft, J.H. Kuypers, and A.P. Pisano, *IEEE Trans. Ultrason. Ferroelectr. Freq. Control* 57, 524 (2010).
36. C.-M. Lin, Y.-Y. Chen, V.V. Felmetsger, W.C. Lien, T. Riekkinen, D.G. Senesky, and A.P. Pisano, *J. Micromech. Microeng.* 23, 025019 (2013).
37. C.-M. Lin, Y.-Y. Chen, V.V. Felmetsger, D.G. Senesky, and A.P. Pisano, *Adv. Mater.* 24, 2722 (2012).